Jyväskylän yliopiston julkaisuarkisto
Jyväskylä University Digital Archive

UNIVERSITY OF JYVÄSKYLÄ

**This is an electronic reprint of the original article.**
**This reprint *may differ* from the original in pagination and typographic detail.**

**Author(s):** Nyman, Markus; Juutinen, Sakari; Darby, Iain; Eeckhaudt, Sarah; Grahn, Tuomas; Greenlees, Paul; Jakobsson, Ulrika; Jones, Peter; Julin, Rauno; Ketelhut, Steffen; Kettunen, Heikki; Leino, Matti; Nieminen, Päivi; Peura, Pauli; Rahkila, Panu; Sarén, Jan; Scholey, Catherine; Sorri, Juha; Uusitalo, Juha; Enqvist, Timo

**Title:** Gamma-ray and decay spectroscopy of 194,195,196At

**Year:** 2013

**Version:**

**Please cite the original version:**

Nyman, M., Juutinen, S., Darby, I., Eeckhaudt, S., Grahn, T., Greenlees, P., Jakobsson, U., Jones, P., Julin, R., Ketelhut, S., Kettunen, H., Leino, M., Nieminen, P., Peura, P., Rahkila, P., Sarén, J., Scholey, C., Sorri, J., Uusitalo, J., & Enqvist, T. (2013). Gamma-ray and decay spectroscopy of 194,195,196At. Physical Review C, 88(5), Article 054320. https://doi.org/10.1103/PhysRevC.88.054320

All material supplied via JYX is protected by copyright and other intellectual property rights, and duplication or sale of all or part of any of the repository collections is not permitted, except that material may be duplicated by you for your research use or educational purposes in electronic or print form. You must obtain permission for any other use. Electronic or print copies may not be offered, whether for sale or otherwise to anyone who is not an authorised user.

# $\gamma$-ray and decay spectroscopy of $^{194,195,196}$At

M. Nyman,[1,*] S. Juutinen,[1] I. Darby,[1,†] S. Eeckhaudt,[1] T. Grahn,[1] P. T. Greenlees,[1] U. Jakobsson,[1] P. Jones,[1,‡] R. Julin,[1] S. Ketelhut,[1,§] H. Kettunen,[1] M. Leino,[1] P. Nieminen,[1] P. Peura,[1] P. Rahkila,[1] J. Sarén,[1] C. Scholey,[1] J. Sorri,[1] J. Uusitalo,[1] and T. Enqvist[2]

[1]*Department of Physics, P.O. Box 35 (YFL), FI-40014 University of Jyväskylä, Finland*

[2]*CUPP, P.O. Box 22, FI-86801 Pyhäsalmi, Finland*

(Received 5 January 2012; revised manuscript received 12 August 2013; published 25 November 2013)

Excited states of $^{195}$At have been studied by means of in-beam $\gamma$-ray spectroscopy and the recoil-decay tagging technique. A strongly coupled rotational band feeding the $\alpha$-decaying $7/2^-$ state via unobserved transitions was identified. This band is presumably built on the oblate proton $I^\pi = 13/2^+$ state. Confirming earlier measurements, $\alpha$ decays from the $1/2^+$ and $7/2^-$ states were observed. Additionally, an $E3$ branch competing with the $\alpha$ decay of the $7/2^-$ state was inferred. Also $\alpha$ decays of the odd-odd isotopes $^{194,196}$At were examined.

DOI: 10.1103/PhysRevC.88.054320 PACS number(s): 23.20.Lv, 21.10.Re, 23.60.+e, 27.80.+w

## I. INTRODUCTION

Neutron-deficient nuclei in the lead region exhibit various shapes coexisting at low excitation energies. The ground states of lead nuclei down to the lightest known isotope are spherical, but both oblate and prolate structures exist in neutron midshell nuclei at low energies [1,2]. Experimental information concerning elements heavier than lead becomes sparser with increasing $Z$ owing to the small production cross sections in fusion-evaporation reactions.

The decrease in excitation energies of the $1/2^+$ and $13/2^+$ states with reducing neutron number is a characteristic feature of odd-$A$ bismuth isotopes (see Fig. 1). These states originate from the proton $(\pi 3s_{1/2})^{-1}$ and $(\pi 1i_{13/2})^{+1}$ configurations, respectively. A strongly coupled rotational band feeding the isomeric $13/2^+$ state has been observed both in $^{193}$Bi and in $^{191}$Bi, indicating an oblate shape [3]. In $^{187,189}$Bi the observed level pattern on top of the $13/2^+$ state suggests a prolate shape [4]. In the lightest odd-$A$ bismuth isotope studied so far, $^{185}$Bi, it has been proposed that a prolate $1/2^+$ state forms the ground state [5].

In odd-$A$ astatine nuclei below the $N = 126$ shell closure the ground state has a spin-parity $9/2^-$ and the configuration $(\pi 1h_{9/2})^3$ down to $^{197}$At [6–13]. In the lighter isotopes $^{191,193,195}$At a $1/2^+$ state associated with a proton 4p-1h intruder configuration becomes the ground state [14,15]. Low-lying isomeric states, stemming from the $1i_{13/2}$ proton orbital, have been previously observed in $^{197,199,201,203}$At [10,12,16] and in $^{193}$At [15]. In $^{193}$At the isomer was even observed to have an $\alpha$-decay branch. The lightest odd-$A$ astatine isotope that has so far been studied by means of in-beam $\gamma$-ray spectroscopy is $^{197}$At, where a strongly coupled rotational band built on the $13/2^+$ state has been reported [13,17].

The decay properties of $^{195}$At were first reported in Refs. [18,19], establishing two $\alpha$-particle energies and half-lives. Later, Enqvist *et al.* performed a more detailed study and found a wide energy distribution for $\alpha$ particles originating from the decay of $^{195}$At [20]. The summing of conversion electron and $\alpha$-particle signals in the implantation detector was proposed as a possible explanation. The latest decay study of $^{195}$At by Kettunen *et al.* confirmed the existence of two $\alpha$-decaying states [14]. The $\pi$(4p-1h) $1/2^+$ state was determined to be the ground state of $^{195}$At and the second $\alpha$-decaying state at 32 keV was assigned a spin and parity of $7/2^-$. The appearance of a low-lying $7/2^-$ state was explained by a change in deformation between $^{197}$At and $^{195}$At: At moderate oblate deformations the 85th proton will occupy the $7/2^-$[514] Nilsson orbital. Prior to the present work only these two states were known in $^{195}$At.

## II. EXPERIMENTAL SETUP

The experiment was carried out at the Accelerator Laboratory of the University of Jyväskylä (JYFL). The $^{195}$At nuclei were produced in the fusion-evaporation reaction $^{147}$Sm($^{51}$V,3n)$^{195}$At and the vanadium ions were accelerated using the $K = 130$ MeV cyclotron. The samarium target foil was 750 $\mu$g/cm$^2$ thick and the beam energy in the middle of the target was 224 MeV. The highly selective recoil-decay tagging (RDT) technique [21–23] was employed in the experiment.

Reaction products recoiling out of the target were separated from the primary beam using the recoil ion transport unit (RITU) gas-filled recoil separator [24] and transported to the GREAT spectrometer [25]. In GREAT they first passed through a multiwire proportional counter (MWPC), which was used to identify fusion-evaporation products based on time-of-flight and energy-loss information. The recoils were then implanted into a highly pixellated double-sided silicon strip detector (DSSD), located at the focal plane of RITU, where their subsequent $\alpha$ decays were observed. The DSSD was surrounded by a box of 28 PIN diode silicon detectors used for the detection of conversion electrons from isomeric transitions.

*Present address: Institute for Reference Materials and Measurements (IRMM), Retieseweg 111, B-2440 Geel, Belgium; markus.e.j.nyman@gmail.com.

†Present address: Instituut voor Kern- en Stralingsfysica, University of Leuven, Celestijnenlaan 200 D, B-3001 Leuven, Belgium.

‡Present address: iThemba LABS, National Research Foundation, P.O. Box 722, Somerset West 7129, South Africa.

§Present address: TRIUMF, 4004 Wesbrook Mall, Vancouver, British Columbia, Canada V6T 2A3.

 ©2013 American Physical Society

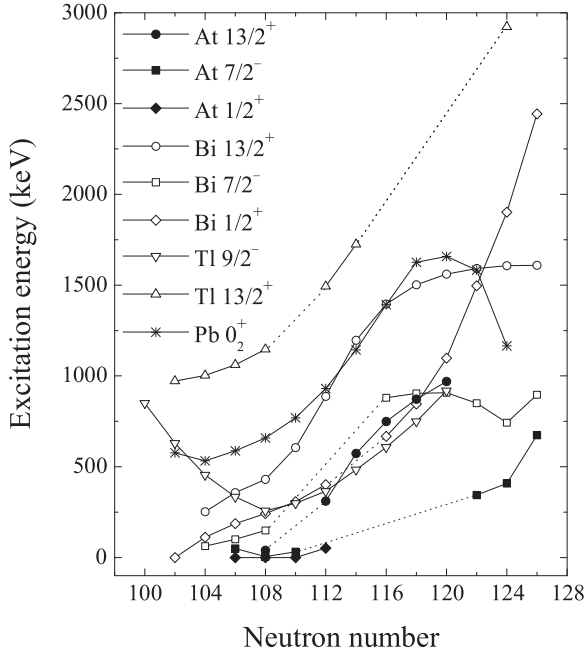


FIG. 1. Energy systematics of various low-lying levels in astatine, bismuth, and thallium isotopes. The neutron number of $^{195}$At is 110.

For $\gamma$-ray detection the GREAT spectrometer was equipped with a planar Ge detector located directly behind the DSSD and a clover Ge detector outside the GREAT vacuum chamber. The planar detector was housed in its own cryostat and included a thin beryllium window to facilitate the observation of low-energy $\gamma$ rays. For the detection of prompt $\gamma$ rays the target chamber was surrounded by 43 Compton-suppressed high-purity Ge detectors making up the JUROGAM array. The total photopeak efficiency of JUROGAM was 4.2% at 1.3 MeV.

Gain matching for the individual strips of the DSSD was carried out using an externally mounted $\alpha$ source containing $^{239}$Pu [$E_\alpha = 5156.59(14)$ keV], $^{241}$Am [$E_\alpha = 5485.56(12)$ keV], and $^{244}$Cm [$E_\alpha = 5804.77(5)$ keV] [26]. The final energy calibration for $\alpha$ particles emitted by recoils implanted into the detector was done using the $^{194}$Po [$E_\alpha = 6842(6)$ keV], $^{195}$Po [$E_\alpha = 6606(5)$ keV, $E_\alpha = 6699(5)$ keV], and $^{196}$Po [$E_\alpha = 6521(5)$ keV] $\alpha$ peaks (see Fig. 2). The $\alpha$-particle energies are taken from Ref. [27].

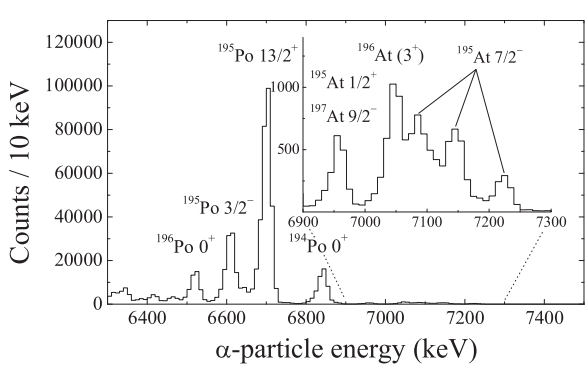


FIG. 2. Recoil-correlated $\alpha$-particle energy spectrum from the reaction $^{51}$V + $^{147}$Sm at 224 MeV in the middle of the target. The recoil-$\alpha$ search time was 4 s. Origin of the three peaks resulting from the decay of the $7/2^-$ state in $^{195}$At is explained in the text. The decay of $^{194}$At forms a wide distribution of events between 7000 and 7300 keV.

The data acquisition system utilized the total data readout (TDR) method, where the use of a hardware trigger and the resulting common dead time have been eliminated [28]. In a TDR system all channels run independently and the necessary correlations and filtering are done in software. A dedicated metronome unit provided the necessary synchronization and time stamping to an accuracy of 10 ns. In on-line and off-line data sorting the GRAIN software was used [29].

## III. RESULTS

### A. $^{195}$At

Recoils implanted into the DSSD were identified by their subsequent $\alpha$ decays. Prompt $\gamma$ rays detected with the JUROGAM array were tagged using appropriate temporal and spatial correlations. The $\alpha$-decay branches of the daughter nucleus ($^{191}$Bi) were sufficient to allow the use of recoil-parent $\alpha$-daughter $\alpha$ correlations. Search times of 4 and 80 s were applied with recoil-parent and parent-daughter correlations, respectively. The total recoil-correlated $\alpha$-particle energy spectrum from the experiment is presented in Fig. 2.

In Ref. [14] the following data are reported: The $7/2^-$ state in $^{195}$At at 32 keV decays via $\alpha$ emission to the $7/2^-$ state in $^{191}$Bi at 149 keV [$E_\alpha = 7075(4)$ keV, $I_{\rm rel} = 95.5(5)\%$] and to the $9/2^-$ ground state [$E_\alpha = 7221(4)$ keV, $I_{\rm rel} = 4.5(5)\%$]. The relative intensities of the two $\alpha$-decay branches were not measured directly owing to conversion electron summing effects explained below. Instead, the intensities quoted above are based on simulations. From the present data set the $\alpha$-particle energies for the two branches originating from the $7/2^-$ state in $^{195}$At were determined to be 7076(5) keV (utilizing coincidences with $\gamma$ rays from the 149 keV $7/2^- \rightarrow 9/2^-$ transition in $^{191}$Bi) and 7222(4) keV. The excitation energy of the $7/2^-$ state was found to be 33(8) keV. These values are in agreement with Ref. [14]. The $\alpha$-decay data from this work for $^{194,195,196}$At and their daughter nuclei $^{190,191,192}$Bi are summarized in Table I. With the exception of $^{194}$At and $^{192}$Bi our results are in a good agreement with literature values. The $\alpha$ decay of odd-odd isotopes is discussed in Sec. III B.

Between the 7076- and 7222-keV peaks the $\alpha$ spectrum is influenced by $\alpha$-electron summing in the DSSD. The peak between those two energies originates from summing of signals coming from the 7076-keV $\alpha$ particles and $K$ conversion electrons from the subsequent 149-keV $M1$ transition ($E_{e,K} \approx 58$ keV). Events between the 7076-keV peak and the sum peak arise from cases where the conversion electron has deposited only part of its energy into the detector. Further contribution comes from $L$ and $M$ conversion electrons. Neither the $7/2^-$ nor the $1/2^+$ $\alpha$-decay events can be cleanly identified in Fig. 2. The energy range containing the $\alpha$ decays from the $7/2^-$ state in $^{195}$At also includes $\alpha$ decays from $^{194}$At. Likewise, the 6953-keV peak is contaminated by $\alpha$ decays from the $9/2^-$ state in $^{197}$At. The presence of $^{197}$At is attributable to the $^{147}$Sm target also containing heavier samarium isotopes as

TABLE I. Decay data for the various At → Bi → Tl decay chains measured in the present work. The group number refers to Fig. 3. The literature values are taken from Refs. [14] ($^{195}$At,$^{191}$Bi), [30] ($^{194}$At), [31] ($^{196}$At), and [32,33] ($^{190,192}$Bi). Groups 5 and 6, weakly visible in Fig. 3, correspond to the same $^{195}$At decays as groups 3 and 4 but are correlated with the $^{191}$Bi $9/2^- \rightarrow {}^{187}$Tl $1/2^+$ daughter decay.

| Group | Nucleus | Decay | $E_\alpha$ (Exp.) | $E_\alpha$ (Lit.) | $t_{1/2}$ (Exp.) | $t_{1/2}$ (Lit.) |
|---|---|---|---|---|---|---|
| 1, 2 | | $1/2^+ \rightarrow 1/2^+$ | 6956(4) | 6953(3) | 290(20) ms | 328(20) ms |
| 3, 5 | $^{195}$At | $7/2^- \rightarrow 7/2^-$ | 7076(5) | 7075(4) | 143(3) ms | 147(5) ms |
| 4, 6 | | $7/2^- \rightarrow 9/2^-$ | 7222(4) | 7221(4) | | |
| 7 | $^{194}$At | Low spin[a] | 7174(8) | 7190 | $240^{+40}_{-30}$ ms | 253(10) ms |
| | | High spin[a] | 7156(5) | 7178 | $300^{+50}_{-40}$ ms | 310(8) ms |
| 8 | $^{196}$At | $(3^+) \rightarrow (3^+)$ | 7047(5) | 7049(4) | $350^{+50}_{-40}$ ms | 388(7) ms |
| 1 | | $1/2^+ \rightarrow 1/2^+$ | 6875(4) | 6870(3) | 114(6) ms | $121^{+8}_{-7}$ ms |
| 2, 3, 4 | $^{191}$Bi | $9/2^- \rightarrow 9/2^-$ | 6315(4) | 6308(3) | 11.7(4) s | 12.4(4) s |
| 5, 6 | | $9/2^- \rightarrow 1/2^+$ | 6641(7) | 6639(5) | | |
| 7 | $^{190}$Bi | $(3^+) \rightarrow (3^+)$ | 6428(6) | 6431(5) | $7.7^{+1.0}_{-0.8}$ s | 6.3(1) s |
| | | $(10^-) \rightarrow (10^-)$ | 6450(5) | 6456(5) | $5.9^{+1.0}_{-0.8}$ s | 6.2(1) s |
| 8 | $^{192}$Bi | $(3^+) \rightarrow (3^+)$ | 6064(5) | 6060(5) | 20(3) s | 34.6(9) s |

[a]See Fig. 8 for a more detailed view of group 7 and Sec. IV B for discussion about the states involved in the decays.

impurities. To unambiguously assign events to the nuclei of interest, recoil-parent $\alpha$-daughter $\alpha$ correlations were used to generate the $\alpha$-$\alpha$ matrix displayed in Fig. 3.

To examine the transitions feeding the known states in $^{195}$At the RDT method was employed. In Fig. 4(a) the total recoil-correlated $\gamma$-ray spectrum from the reaction $^{51}$V + $^{147}$Sm is displayed. It is dominated by transitions in the most abundant reaction products, $^{194,195,196}$Po. In Fig. 4(b) a $\gamma$-ray spectrum with the additional condition of an $\alpha$ decay from the $7/2^-$ state in $^{195}$At observed within 450 ms from recoil implantation is presented. Figure 4(c) shows a $\gamma$-ray spectrum tagged in the same manner with the $\alpha$ decays from the $1/2^+$ ground state of $^{195}$At (1 s recoil-$\alpha$ search time). The $\gamma$ rays assigned to $^{195}$At are listed in Table II and the deduced level scheme is presented in Fig. 5.

A $\gamma$-$\gamma$ matrix tagged with $\alpha$ decays from the $7/2^-$ state was also made and coincidence analysis was carried out using the RADWARE software package [34,35]. A strongly coupled band was constructed based on coincidences as well as energy-sum and intensity arguments (band 1 in Fig. 5). In spite of the limited statistics the $M1$ transitions can be seen in coincidence with each other. The level structure is similar to those observed on top of the isomeric $13/2^+$ states in neighboring odd-$Z$ nuclei. Therefore, the band head is assigned with $I^\pi = (13/2^+)$ and the $1i_{13/2}$ configuration. In heavier odd-$A$ At nuclei the $1i_{13/2}$ bandhead is depopulated by an $M2$ transition to the $9/2^-$ ground state. In $^{195}$At the $9/2^-$ state has not been observed and the $(13/2^+)$ band feeds the $7/2^-$ level. Band 1 is therefore seen when tagging with the $\alpha$ decays of the $7/2^-$ state. As discussed later in this article, the deexcitation path of the $(13/2^+)$ state remains unobserved. The 439-keV $\gamma$ ray appears in coincidence with the 281-keV transition only, which is why it is placed to feed the $(15/2^+)$ state.

Transitions not appearing in coincidence with those assigned to the yrast band presumably feed the $7/2^-$ state. Based on its high intensity the 302.8-keV $\gamma$ ray is a strong candidate to be placed directly above the $7/2^-$ state. Unfortunately, no unambiguous coincidence relationships could be found from the present data. Therefore, the level structure directly above the $7/2^-$ state remains unresolved. In addition to the 302.8-keV transition the $\gamma$ rays with energies of 416.2, 420.6, 434.4, 496.1, and 499.1 keV are good candidates to feed the $7/2^-$ state. To confirm the assignment of $\gamma$ rays to $^{195}$At, a recoil-$\alpha$-$\alpha$ tagged $\gamma$-ray spectrum was made (prompt $\gamma$ rays correlated with groups 3–6 in Fig. 3). This provided a clean spectrum, albeit with low statistics. The $\gamma$ rays feeding the $7/2^-$ state, which were finally included in Table II, were required to be present also in this spectrum.

A $\gamma$-ray spectrum tagged with the $1/2^+$ ground-state $\alpha$ decays of $^{195}$At is presented in Fig. 4(c). The number of observed $\alpha$ particles from the $1/2^+$ state was only about 2000; hence, the low statistics in the $\gamma$-ray spectrum. Nonetheless, it is clear that the strongest lines present in the spectrum tagged with the $7/2^-$ $\alpha$ decays are also seen here (indicated with dotted lines). This implies that there is a link between the $7/2^-$ and the $1/2^+$ states. The half-life for a $7/2^- \rightarrow 1/2^+$ $E3$ transition would be such that it could compete with the $\alpha$ decay of the $7/2^-$ state. This $E3$ branch is discussed in the next paragraph. Also present in Fig. 4(c) are $\gamma$ rays from $^{197}$At owing to overlapping $\alpha$-particle energies. After excluding the contaminant $\gamma$ lines, the remaining transitions are assigned to feed the $1/2^+$ state in $^{195}$At. The proposed level structure (band 2 in Fig. 5) is only based on energy sum and intensity arguments, as the statistics is insufficient for $\gamma$-$\gamma$ coincidence analysis. Therefore, the placement of levels in band 2 is tentative.

There is indirect evidence for a $1/2^+ \rightarrow 7/2^-$ $E3$ transition in $^{189,191}$Bi [14,15]. In $^{195}$At the $7/2^-$ state lies above the $1/2^+$ state, but the $7/2^- \rightarrow 1/2^+$ $E3$ transition has not been observed. As the 33-keV transition is highly converted, detection of $\gamma$ rays is out of the question. Also the conversion electrons have energies that are too low to be observed in the present experiment. However, the $E3$ branch can be determined from the recoil-$\alpha$ time distribution of the decay

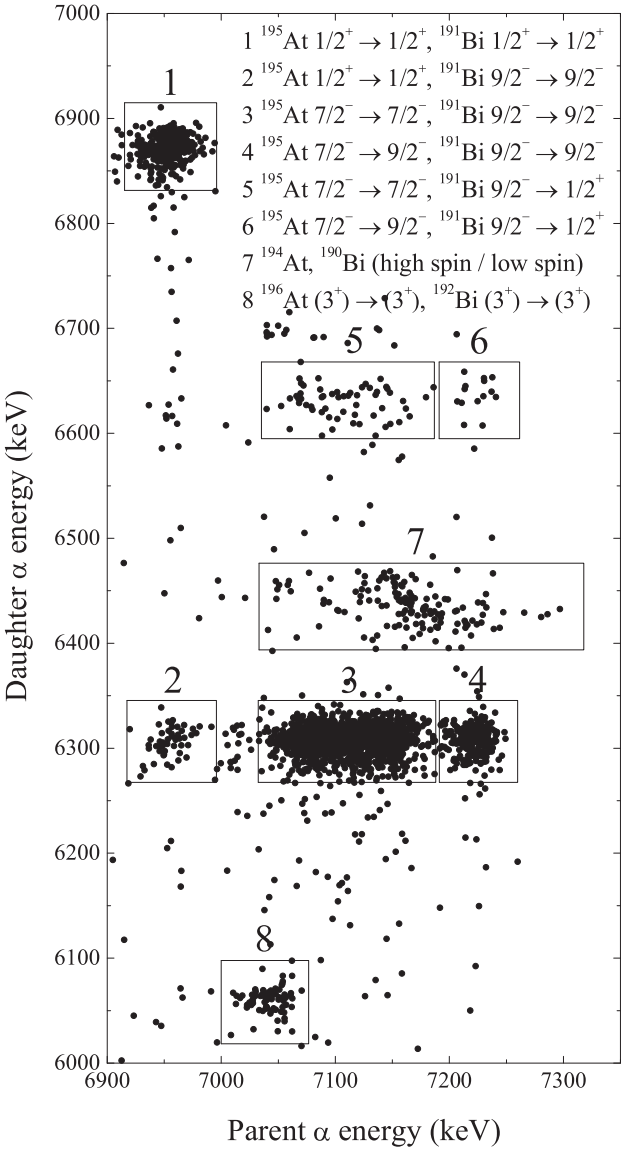


FIG. 3. Recoil-correlated $\alpha$-$\alpha$ matrix from the reaction $^{51}$V + $^{147}$Sm. Initial and final states for both parent and daughter decays are indicated in the figure.

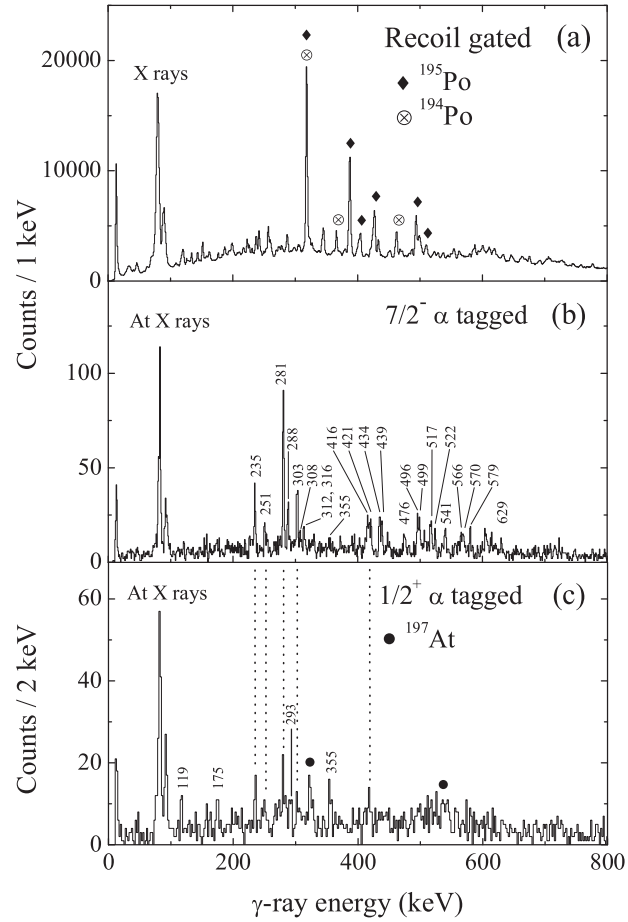


FIG. 4. (a) Total recoil gated $\gamma$-ray spectrum from the present experiment. (b) $\gamma$-ray spectrum tagged with the $\alpha$ decays of the $7/2^-$ state in $^{195}$At. (c) $\gamma$-ray spectrum tagged with the $\alpha$ decays of the $1/2^+$ ground state.

of the $1/2^+$ state. Time spectra for both $1/2^+$ and $7/2^-$ state $\alpha$ decays are presented in Fig. 6. To sufficiently reduce the background, $\alpha$-$\alpha$ correlations were required (groups 1–6 in Fig. 3). The half-life of the $7/2^-$ state was first determined to be 143(3) ms. Then a fit, where the two components contributing to the decay of the $1/2^+$ state were taken into account, was used to find out the $E3$ branch and the half-life of the $1/2^+$ state. The contribution through the $E3$ branch to the population of the $1/2^+$ state (from the fit) was used to determine the $E3$ branching ratio for the $7/2^-$ state. A value of $b_{E3} = 12(4)\%$ was obtained. The half-life of the $1/2^+$ state, also extracted from the fit, was 290(20) ms. The presence of $\gamma$ rays feeding the $(13/2^+)$ and $7/2^-$ states in the $1/2^+$ $\alpha$-tagged spectrum [indicated with dotted lines in Fig. 4(c)] makes it possible to confirm the result for the $E3$ branching ratio. The intensities of these peaks, when compared to the $7/2^-$ $\alpha$-tagged spectrum [Fig. 4(b)], give a value of $b_{E3} = 13(6)\%$, which is in very good agreement with the result obtained from the recoil-$\alpha$ time distribution.

Transitions deexciting the $(13/2^+)$ state in $^{195}$At were searched from the focal plane data to pin down the excitation energy of this state. In $^{197}$At the $13/2^+$ state has a half-life of 1.3(2) $\mu$s and it decays via a 310.7-keV $M2$ transition to the $9/2^-$ ground state [17]. In $^{193}$At the $13/2^+$ state at an excitation energy of 39(7) keV decays mainly via an $E3$ transition to the $7/2^-$ state at 5(10) keV [15]. Based on systematics the $13/2^+$ state in $^{195}$At is expected to be located below 200 keV in excitation energy (see Fig. 1).

Three different scenarios regarding the possible decay modes of the $(13/2^+)$ state were considered. In the first case the situation would be similar to that observed in $^{193}$At and the decay would proceed via two competing processes: an $E3$ transition to the $7/2^-$ state and an $\alpha$ decay to the $13/2^+$ state in $^{191}$Bi. This is the only case involving an $\alpha$-decay branch for the $13/2^+$ state. Another option would be an $M2$ transition to an unobserved $9/2^-$ level in $^{195}$At. This would then be followed by an $M1$ transition to the $7/2^-$ state. Finally, should the $(13/2^+)$ level lie sufficiently high in energy, it would be

TABLE II. $\gamma$-ray transitions assigned to $^{195}$At.

| $E_\gamma$ (keV) | $I_\gamma$ | $E_i$ (keV) | $I_i^\pi$ | $I_f^\pi$ |
|---|---|---|---|---|
| 119.2(5) | 10(3) | [119.2(5)] | | $1/2^+$ |
| 175.2(5) | 7(3) | [293.6(7)] | $(5/2^+)$ | |
| 235.1(4) | 35(9) | $\Delta+$ 516.6(5) | $(17/2^+)$ | $(15/2^+)$ |
| 250.8(7) | 25(9) | $\Delta+$ 1056.7(9) | $(21/2^+)$ | $(19/2^+)$ |
| 281.2(2) | 100(15) | $\Delta+$ 281.2(3) | $(15/2^+)$ | $(13/2^+)$ |
| 288.4(4) | 36(10) | $\Delta+$ 804.2(7) | $(19/2^+)$ | $(17/2^+)$ |
| 293.0(6) | 8(4) | [293.6(7)] | $(5/2^+)$ | $1/2^+$ |
| 302.8(3)[a] | 58(12) | | | |
| 307.5(7)[a] | 17(9) | | | |
| 312.3(9)[a] | 19(12) | | | |
| 315.5(15) | 12(10) | $\Delta+$ 1371.1(12) | $(23/2^+)$ | $(21/2^+)$ |
| 355.2(7) | 12(5) | [649.6(13)] | $(9/2^+)$ | $(5/2^+)$ |
| 416.2(6)[a] | 35(12) | | | |
| 420.6(5)[a] | 43(12) | | | |
| 434.4(5)[a] | 40(12) | | | |
| 438.6(6) | 34(12) | $\Delta+$ 719.8(7) | | $(15/2^+)$ |
| 476.2(7)[a] | 25(11) | | | |
| 496.1(6)[a] | 28(8) | | | |
| 499.1(8)[a] | 28(8) | | | |
| 517.1(6) | 33(13) | $\Delta+$ 516.6(5) | $(17/2^+)$ | $(13/2^+)$ |
| 522.4(6) | 29(11) | $\Delta+$ 804.2(7) | $(19/2^+)$ | $(15/2^+)$ |
| 541.0(5) | 34(11) | $\Delta+$ 1056.7(9) | $(21/2^+)$ | $(17/2^+)$ |
| 566.5(8) | 40(20) | $\Delta+$ 1371.1(12) | $(23/2^+)$ | $(19/2^+)$ |
| 569.9(8)[a] | 40(20) | | | |
| 579.4(8) | 21(12) | $\Delta+$ 1635(2) | $(25/2^+)$ | $(21/2^+)$ |
| 629.2(5)[a] | 34(12) | | | |

[a]Observed in the $7/2^-$ $\alpha$-tagged spectrum but not placed in the level scheme.

possible for it to decay via an $E1$ transition to an $11/2^-$ state above the $7/2^-$ level.

An extensive search was undertaken to observe $\alpha$ particles, $\gamma$ rays, or conversion electrons originating from the decay of the $(13/2^+)$ state. We consider the $E1$ decay mode first. The $11/2^-$ state with a mixed $(\pi 1h_{9/2}/\pi 2f_{7/2})$ configuration has been placed at 655 keV in $^{199}$At and at 505 keV in $^{197}$At [13]. The $11/2^-$ states in odd-$A$ Bi isotopes follow a very similar trend. Based on these

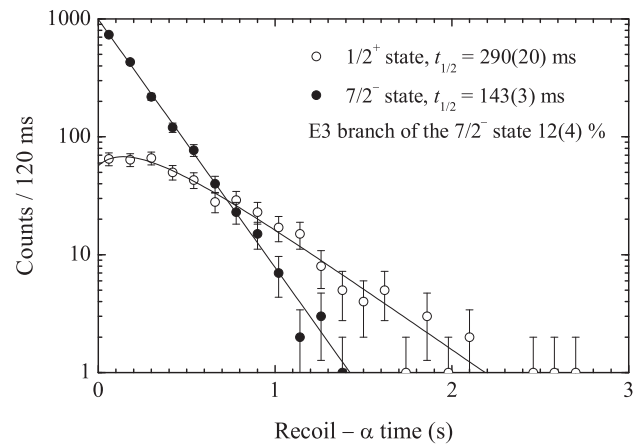


FIG. 6. Recoil-$\alpha$ time distributions for the $1/2^+$ and $7/2^-$ states. The half-lives and the $E3$ branching ratio were extracted from the fitted decay curves (see text for details).

systematics the $11/2^-$ state in $^{195}$At would be expected to lie around 350 keV. This is already considerably higher than the expected excitation energy of the $(13/2^+)$ state $[E(13/2^+) < 200$ keV$]$. If the $(13/2^+)$ state would lie above the $11/2^-$ level, it seems therefore reasonable to expect the energy of the $E1$ transition to be quite low. The $13/2^+ \rightarrow 11/2^-$ $E1$ transition would also be hindered. The $E1$ transition strength has been estimated to be $7.5 \times 10^{-6}$ W.u. in the case of $^{197}$Bi [36]. With this value one obtains a half-life of $t_{1/2} > 25$ ns for the $(13/2^+)$ level in $^{195}$At, assuming $E_{E1} < 100$ keV. In this case the $E1$ transition would remain unobserved in the present experiment as the $\gamma$ rays would go undetected during the flight through the recoil separator. Higher energy $E1$ transitions would have half-lives short enough to be observed in the prompt $\gamma$-ray spectra, but this would place the energy of the $(13/2^+)$ state unrealistically high. In conclusion, the $E1$ decay mode for the $(13/2^+)$ state is considered unlikely based on energy level systematics, although its existence cannot be entirely ruled out in the present experiment.

The scenario involving an $\alpha$ decay or an $E3$ transition would be observable in the focal plane detectors owing to

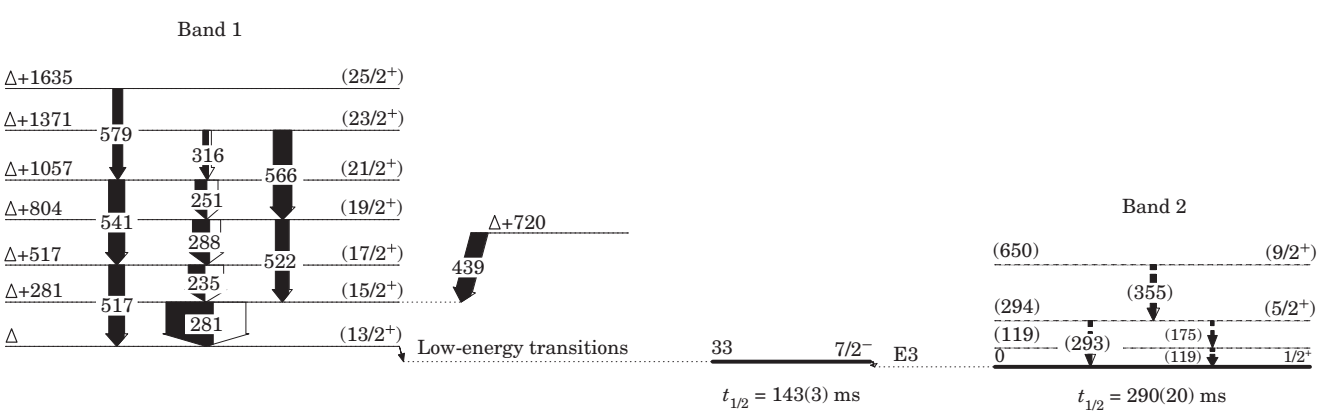


FIG. 5. Level scheme of $^{195}$At. An upper limit for the $(13/2^+)$ state excitation energy was estimated to be about $\Delta \sim 130$ keV (see text for details).

the longer half-life of the $(13/2^+)$ state. However, it can be ruled out owing to nonobservation of suitable recoil-$\alpha$-$\alpha$ or recoil-$\alpha$-electron/$\gamma$ type events.

The remaining option, where the $(13/2^+)$ state decays to the $7/2^-$ state via an intermediate $9/2^-$ level, was investigated by studying recoil-electron/$\gamma$-$\alpha$-type events. Again, nothing was found that could be attributed to the decay of the $(13/2^+)$ state. However, this decay mode could not be ruled out as it is possible that the transitions have such a low energy that they lie below the detection thresholds of the current experimental system. If one assumes a decay path involving an $M2$ transition followed by an $M1$ and makes use of the estimated efficiencies of the focal plane detectors from Ref. [37], limits can be placed on the transition energies that would lead to observable events (conversion electrons from an $M2$ transition or $\gamma$ rays from an $M1$ transition). Upper limits of $E_{M2} < 65$ keV and $E_{M1} < 30$ keV can be deduced. This would place the $(13/2^+)$ state somewhere below 130 keV in excitation energy.

An $E3$ branch from the $1/2^+$ state to the $7/2^-$ state in $^{191}$Bi was reported in Ref. [14]. Its existence was confirmed in the present work and the branching ratio was determined from $\alpha$-$\alpha$ correlated events. The result was $b_{E3} = 22(6)\%$, in reasonable agreement with the previous value, $b_{E3} = 32(5)\%$. The strength of the $E3$ transition is approximately 0.08 W.u., which is very similar to the strength of the $7/2^- \rightarrow 1/2^+$ $E3$ transition in $^{195}$At determined from the present data (0.07 W.u.). The $\alpha$-decay scheme of $^{195}$At from this experiment is displayed in Fig. 7.

The production cross section of $^{195}$At in the reaction $^{147}$Sm($^{51}$V,3$n$)$^{195}$At at a bombarding energy of 224 MeV in the middle of the target was estimated to be 1.2 $\mu$b, based on the number of recoil-$\alpha$-$\alpha$ correlated events.

### B. Odd-odd isotopes $^{194,196}$At

The isotopes $^{196}$At and $^{194}$At were produced in the $2n$ and $4n$ evaporation channels of the $^{51}$V + $^{147}$Sm reaction,

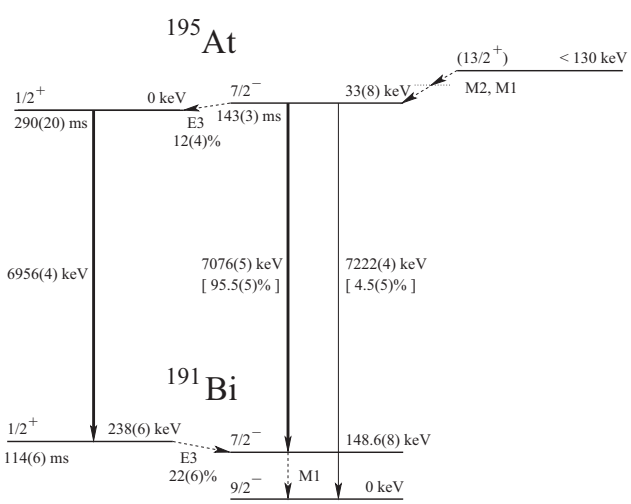


FIG. 7. Decay scheme of $^{195}$At from the present experiment. The relative intensities of the $\alpha$ decays from the $7/2^-$ level in $^{195}$At cannot be measured directly owing to electron summing effects. The intensities included here, from Ref. [14], are based on simulations.

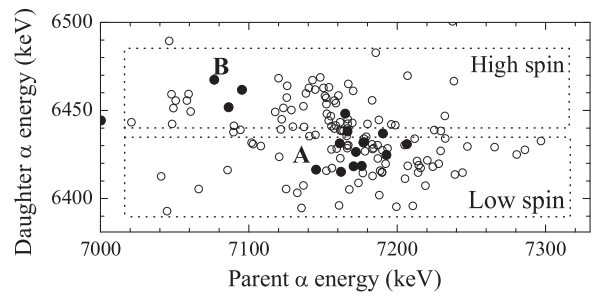


FIG. 8. A part of the $\alpha$-$\alpha$ matrix (Fig. 3) showing the events originating from the decay of $^{194}$At. All observed decays are displayed with open circles, while the solid circles represent $^{194}$At $\alpha$ decays followed by a 70–80-keV $\gamma$ ray in prompt coincidence.

respectively. A typical feature of odd-odd nuclei in this region is the existence of $\alpha$-decaying high-spin and low-spin states ($I^\pi = 10^-, 3^+$). The $\alpha$ decay of $^{194}$At was recently studied in detail and a decay scheme identifying two $\alpha$-decaying states and eight $\alpha$-decay energies was presented [30]. In $^{196}$At only one $\alpha$ decaying state has been observed [31].

The decays of $^{194}$At can be identified by correlating with $\alpha$ decays from the $(3^+)$ [$E_\alpha = 6431(5)$ keV] and $(10^-)$ [$E_\alpha = 6456(5)$ keV] states in the $^{190}$Bi daughter nucleus [32,33]. As the daughter $\alpha$-particle energies are very close to each other, the events in the $\alpha$-$\alpha$ matrix end up in two partially overlapping groups (see Fig. 8). A rough division between events belonging mostly to the low-spin and high-spin decays was made using the following energy conditions for the daughter $\alpha$ decays: $6390 < E_\alpha < 6435$ and $6440 < E_\alpha < 6485$. The most prominent peak in the high-spin part, taken from the projection of events within the high-spin boundaries to the $x$ axis, corresponds to an energy of 7156(5) keV. Similarly, in the low-spin part the largest peak has an energy of 7177(5) keV. The corresponding values reported in Ref. [30] are 7178 and 7190 keV, respectively. The difference compared to the energies obtained here has no clear explanation, but obviously the limited statistics in the present experiment can play a role.

The $\gamma$-ray events following the $\alpha$ decay of $^{194}$At reveal only one peak at 76.7(3) keV. The associated parent $\alpha$-decay events have an energy of $E_\alpha = 7174(8)$ keV (group A in Fig. 8). The number of coincident $\gamma$ rays compared to the total number of $\alpha$ particles within group A is consistent with an $E1$ multipolarity. The energy of the daughter $\alpha$ decay is $E_\alpha = 6428(6)$ keV, compatible with the literature value for the decay of the low-spin isomer in $^{190}$Bi. A 76-keV $E1$ transition is also discussed in Ref. [30]. However, the reported energy for the corresponding $\alpha$ particle is somewhat larger, $E_\alpha = 7190$ keV. A small group of $\alpha$-decay events [$E_\alpha = 7086(13)$ keV] coincident with $\gamma$ rays of similar energy [$E_\gamma = 75(1)$ keV] is observed following the decay of the high-spin isomer in $^{194}$At (group B in Fig. 8). The level of statistics does not allow solid conclusions to be drawn.

The relative population of the high-spin and low-spin isomers in the present experiment can also be evaluated. Taking into account the respective $\beta$-decay branches for the daughter nuclei the ratio between the population of the high-spin isomer to the total is $N(\text{high})/N(\text{total}) = 37(15)\%$ in $^{194}$At.

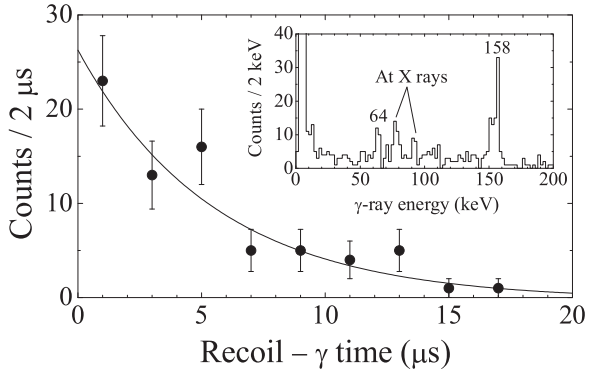


FIG. 9. Time distribution between recoil formation and the observation of a 157.5-keV $\gamma$ ray in the planar Ge detector. An exponential fit is shown as the solid line [$t_{1/2} = 4.0(7)$ $\mu$s]. The energy spectrum of delayed $\gamma$ rays, tagged with the $^{196}$At $\alpha$ decays and recorded with the planar Ge detector, is shown in the inset. The low-energy tail seen clearly in the 157.5-keV peak is attributable to poor energy resolution of the detector and does not indicate the presence of another peak. The recoil-$\gamma$ search time was 100 $\mu$s.

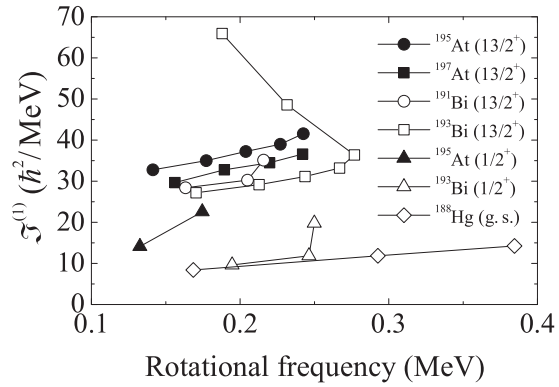


FIG. 10. Kinematic moment of inertia plotted against rotational frequency for bands 1 and 2 in $^{195}$At and for similar bands in $^{197}$At [13] and $^{191,193}$Bi [3]. The low-spin part of the weakly deformed ground-state band in $^{188}$Hg is also shown for comparison [38].

For $^{196}$At a total of 89 recoil-parent $\alpha$-daughter $\alpha$ events were collected during the experiment. The $\alpha$-decay properties determined from these data are summarized in Table I. It appears that the only $\alpha$-decaying state present in $^{196}$At is the low-spin ($3^+$) level. The half-life obtained in the present work for the ($3^+$) decay in $^{192}$Bi [20(3) s] is shorter than the literature value [34.6(9) s]. This could be attributable to random correlations present owing to the long parent-daughter search time.

An isomeric state in $^{196}$At with a half-life of 7.6(1.4) $\mu$s and decaying via a 157.9(1)-keV $E2$ transition was reported in Ref. [31]. This transition was confirmed in the present experiment and the energy was measured to be $E_\gamma = 157.5(9)$ keV. The associated $\gamma$-ray energy spectrum and recoil-$\gamma$ time distribution are presented in Fig. 9. The half-life of 4.0(7) $\mu$s, determined from an exponential fit, is shorter than the one previously reported. Based on the number of observed $\gamma$ rays and assuming an $E2$ multipolarity, the intensity of the 157.5-keV transition, normalized to the total number of $^{196}$At $\alpha$ decays, is $N(157.5)/N(\text{total}) = 43(7)\%$. In addition to the 157.5-keV line and astatine $K$ x rays, a 64(1)-keV $\gamma$ ray is also observed. The corresponding half-life is 11(3) $\mu$s, indicating that it lies in the level scheme below the 157.5-keV transition, or that it belongs to a different cascade. Placements of these transitions in the decay scheme cannot be deduced from the present data.

Finally, approximate values for the production cross sections of $^{194,196}$At in the reaction $^{51}$V + $^{147}$Sm were estimated, based on recoil-$\alpha$-$\alpha$ correlated events. The results were $\sigma \approx 50$ nb for $^{194}$At and $\sigma \approx 230$ nb for $^{196}$At at a beam energy of 224 MeV in the middle of the target.

## IV. DISCUSSION

### A. $^{195}$At

Total Routhian surface (TRS) calculations presented in Ref. [17] predict a nearly spherical minimum for the $(1h_{9/2})^3$ proton configuration in odd-$A$ $^{197-211}$At isotopes. The deformations of these minima increase with decreasing mass to about $\beta_2 \approx 0.1$, $\gamma \approx 0^\circ$ in $^{197}$At. A sharp change occurs between $^{197}$At and $^{195}$At, where the nucleus adopts an oblate shape ($\beta_2 \approx 0.2$) with the odd proton now occupying the $7/2^-$[514] Nilsson orbital. This is confirmed by the observation of low-lying $I^\pi = 7/2^-$ states in $^{191,193,195}$At [14,15]. In the present work it was not possible to determine the level structure on top of the $7/2^-$ state in $^{195}$At. A strongly coupled band might be expected, as such a band is observed in its $\alpha$-decay daughter nucleus, $^{191}$Bi. A collective near-oblate minimum for the $1i_{13/2}$ proton configuration is predicted to lie at $\beta_2 \approx 0.2$, $\gamma \approx -50^\circ$. The rotation of an oblate nucleus with this configuration would result in a strongly coupled band, as confirmed by our experiment (band 1 in Fig. 5). For the $(3s_{1/2})^{-1}$ proton configuration a collective triaxial minimum at $\beta_2 \approx 0.17$, $\gamma \approx -40^\circ$ is predicted by the TRS calculations. This would give rise to a decoupled rotational band.

The yrast band in $^{195}$At is assigned a $\pi 1i_{13/2}$ configuration. Similar strongly coupled bands based on the same configuration have been observed in $^{197}$At [17] as well as in $^{191,193}$Bi [3]. In Fig. 10 the kinematic moment of inertia is plotted as a function of rotational frequency for bands 1 and 2 in $^{195}$At. Data for similar bands in $^{197}$At and $^{191,193}$Bi are included for comparison. In the case of the $1i_{13/2}$ bands there is a clear trend of increasing moment of inertia, indicative of increased deformation, when moving further towards the neutron midshell in both Bi and At isotopes. The backbend observed in $^{193}$Bi is a sign of an alignment of a pair of $1i_{13/2}$ neutrons. The bands in the astatine isotopes are not observed to sufficiently high rotational frequencies for potential backbending to emerge.

The kinematic moment of inertia for band 2 in $^{195}$At is larger than that of the $1/2^+$ band in $^{193}$Bi. The low-spin part of the weakly oblate deformed ground-state band in $^{188}$Hg is also included in Fig. 10 [38]. Deformation of the ground state in $^{188}$Hg is determined to be $\beta_2 \approx 0.15$ [39]. Figure 10 seems to indicate that the $1/2^+$ state in $^{193}$Bi has a weakly deformed oblate shape, whereas there is a change to a larger deformation in $^{195}$At. Whether band 2 is a part of a decoupled

structure feeding the $1/2^+$ state cannot be firmly concluded with the level of statistics obtained in this experiment.

### B. $^{194,196}$At

Interpreting experimental data of the odd-odd At isotopes is greatly complicated owing to the high level density encountered in these nuclei. The odd proton and neutron couple their angular momenta to form a multiplet of states with spins $|I_p - I_n| \leqslant I \leqslant I_p + I_n$. Coupling rules for determining the level ordering within the multiplet are given in Refs. [40–42]. Energy of the lowest state in a given multiplet can be estimated by summing the energies of the relevant proton and neutron orbitals in the neighboring odd-even and even-odd nuclei. To test this approach, the energy difference between $(\pi 1h_{9/2} \otimes \nu 1i_{13/2})10^-$ and $(\pi 3s_{1/2}^{-1} \otimes \nu 1i_{13/2})7^+$ levels, estimated in the manner explained above, was compared to experimental data in odd-odd $^{186-192}$Tl nuclei. The energy difference was reproduced within about ±20 keV. Unfortunately experimental data for such comparisons is not available in the case of odd-odd Bi and At isotopes. Figure 11 shows the estimated level energies for some low-lying states in several odd-odd astatine isotopes. Additionally, experimental $\alpha$-decay systematics for odd-odd At nuclei are displayed in Fig. 12, along with some calculated $\alpha$-particle energies for various possible favored decays relevant for the following discussion. The calculated values were obtained by estimating the excitation energies of the states involved in the parent and daughter nuclei using the simple method outlined above. The corresponding $\alpha$-particle energies were then calculated using the experimental energies for ground-state-to-ground-state decays in odd-odd astatine isotopes, assuming that the low-spin isomer remains the ground state down to $^{192}$At.

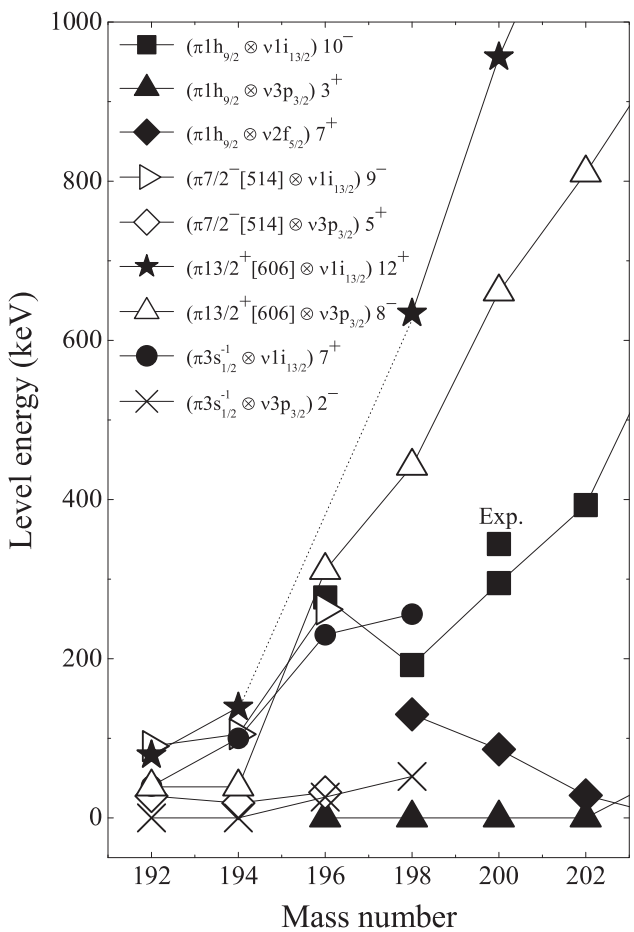


FIG. 11. Estimated level energies for the lowest members of some proton-neutron multiplets occurring in odd-odd astatine isotopes. The method for computing the energies is explained in the text. One experimental data point that was available for $^{200}$At is included for comparison [43].

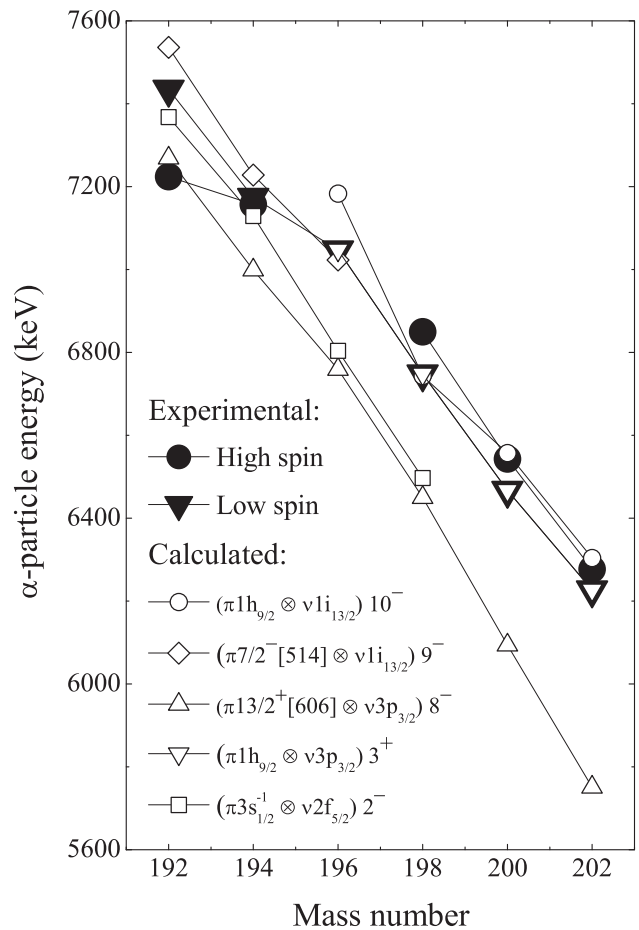


FIG. 12. Energy systematics for $\alpha$ decays of odd-odd astatine isotopes. In addition to experimental data, calculated values for favored $\alpha$ decays of various configurations are included (see text for details).

The absence of an $\alpha$ decay from the high-spin isomer in $^{196}$At can be understood by considering the possible configurations expected to be found at low excitation energies (see Fig. 11). Oblate $(\pi 7/2^-[514] \otimes \nu 1i_{13/2})$ and $(\pi 13/2^+[606] \otimes \nu 3p_{3/2})$ configurations with spin-parities $9^-$ (or $10^-$) and $8^-$, respectively, are likely to come below the spherical $10^-$ state. An oblate $(\pi 3s_{1/2}^{-1} \otimes \nu 1i_{13/2})7^+$ level is expected, in addition to the spherical $(\pi 1h_{9/2} \otimes \nu 2f_{5/2})7^+$ state, to lie at low excitation energy and be located below the $9^-$ (and $8^-$) states. Furthermore, a $(\pi 7/2^-[514] \otimes \nu 3p_{3/2})5^+$ level should also be present at low energy. Thus, the $9^-$ state in $^{196}$At

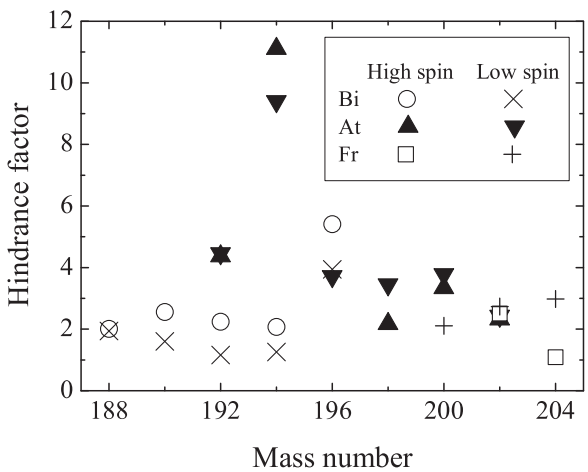


FIG. 13. Hindrance factors for $\alpha$ decays of some odd-odd Bi, At, and Fr isotopes, calculated using the Taagepera-Nurmia formula [45]. The anomalous situation present in $^{194}$At is very evident. Data are taken from Refs. [30–33,43,44,46–48].

could deexcite via an $M2$ transition to either one of the $7^+$ states, with $\Delta I \leqslant 2$ transitions to the ground state following. As a result, the only $\alpha$-decaying state in $^{196}$At would be the $(\pi 1h_{9/2} \otimes \nu 3p_{3/2})3^+$ level. The observed 157.5-keV $E2$ $\gamma$-ray transition could be a part of this internal decay path from the $9^-$ state to the ground state, its half-life being determined by the preceding $9^- \rightarrow 7^+$ $M2$ transition. The measured half-life for the 157.5-keV transition, 4.0(7) $\mu$s, is consistent with the Weisskopf estimate for an approximately 50-keV $M2$ transition, which would remain unobserved in the present experiment.

In $^{194}$At the ground state does not necessarily have a spin parity of $3^+$, because the favored $\alpha$ branch is followed by an $E1$ transition. As can be seen from Figs. 11 and 12, the $\alpha$-decaying low-spin state in $^{194}$At may be the $I^\pi = 2^-$ state originating from the $(\pi 3s_{1/2}^{-1} \otimes \nu 3p_{3/2})$ configuration. The 76.7-keV $E1$ $\gamma$ ray observed to follow the $\alpha$ decay would then naturally be explained as a $2^- \rightarrow 3^+$ transition in $^{190}$Bi.

The $(\pi 1h_{9/2} \otimes \nu 1i_{13/2})10^-$ state in $^{194}$At is expected to lie even higher in energy than the one in $^{196}$At and also would not decay by $\alpha$ emission. Contrary to $^{196}$At, the $(\pi 1h_{9/2} \otimes \nu 2f_{5/2})7^+$ and $(\pi 3s_{1/2}^{-1} \otimes \nu 1i_{13/2})7^+$ states in $^{194}$At possibly lie above the $9^-$ (and $8^-$) levels, thus removing the deexcitation path via electromagnetic transitions. The $\alpha$ decay from the high-spin state in $^{194}$At is also hindered, as can be seen from Fig. 13, where hindrance factor systematics for $\alpha$ decays observed in various odd-odd Bi, At, and Fr isotopes are shown.

Also the $\alpha$ decay of $^{192}$At has been observed not to feed directly the $(3^+)$ and $(10^-)$ states in the daughter nucleus $^{188}$Bi, as reported in Ref. [44]. The energy of the unhindered $\alpha$ decay from the high-spin isomer is considerably lower that what would be expected based on the corresponding energies in heavier odd-odd At nuclei (see Fig. 12). This means that the decay involves a configuration that is at much lower energy in the parent nucleus than in the daughter nucleus. This points to the involvement of the proton $1i_{13/2}$ configuration (see Fig. 1). We therefore propose that the $\alpha$-decaying high-spin isomer in $^{192}$At has the configuration $(\pi 13/2^+[606] \otimes \nu 3p_{3/2})8^-$.

## V. CONCLUSIONS

For the first time $\gamma$-ray transitions were observed in the very neutron-deficient nucleus $^{195}$At. A strongly coupled rotational band based on an oblate $(13/2^+)$ state was found. The energy of the bandhead could not be determined as its decay path remained unobserved. However, using information on the detection thresholds and efficiencies of the experimental setup, an upper limit of about 130 keV was deduced for the excitation energy of the $(13/2^+)$ level. The decay paths and half-lives of the $1/2^+$ and $7/2^-$ states were investigated and a $7/2^- \rightarrow 1/2^+$ $E3$ transition was inferred. Also, the $\alpha$ decays of odd-odd isotopes $^{194,196}$At were studied and possible configurations for the low-spin and high-spin isomers were discussed.

## ACKNOWLEDGMENTS

We thank the personnel at the Accelerator Laboratory of the University of Jyväskylä. This work has received support through EURONS (European Commission Contract No. RII3-CT-2004-506065) and from the Academy of Finland under the Finnish Centre of Excellence Programme 2006–2011 (Nuclear and Accelerator Based Physics Contract No. 213503). We would also like to thank the UK/France (STFC/IN2P3) detector Loan Pool and GAMMAPOOL European Spectroscopy Resource for the detectors used in the JUROGAM array. P.N. acknowledges funding from the Academy of Finland (Contract No. 121110).

[1] K. Heyde, P. Van Isacker, M. Waroquier, J. L. Wood, and R. A. Meyer, Phys. Rep. **102**, 291 (1983).
[2] J. L. Wood, K. Heyde, W. Nazarewicz, M. Huyse, and P. V. Duppen, Phys. Rep. **215**, 101 (1992).
[3] P. Nieminen *et al.*, Phys. Rev. C **69**, 064326 (2004).
[4] A. Hürstel *et al.*, Eur. Phys. J. A **21**, 365 (2004).
[5] A. N. Andreyev, D. Ackermann, F. P. Heßberger, K. Heyde, S. Hofmann, M. Huyse, D. Karlgren, I. Kojouharov, B. Kindler, B. Lommel, G. Münzenberg, R. D. Page, K. Van de Vel, P. Van Duppen, W. B. Walters, and R. Wyss, Phys. Rev. C **69**, 054308 (2004).
[6] I. Bergström, B. Fant, C. J. Herrlander, P. Thieberger, K. Wikström, and G. Astner, Phys. Lett. B **32**, 476 (1970).
[7] T. P. Sjoreen, G. Schatz, S. K. Bhattacherjee, B. A. Brown, D. B. Fossan, and P. M. S. Lesser, Phys. Rev. C **14**, 1023 (1976).
[8] T. P. Sjoreen, U. Garg, and D. B. Fossan, Phys. Rev. C **23**, 272 (1981).
[9] T. P. Sjoreen, D. B. Fossan, U. Garg, A. Neskakis, A. R. Poletti, and E. K. Warburton, Phys. Rev. C **25**, 889 (1982).
[10] K. Dybdal, T. Chapuran, D. B. Fossan, W. F. Piel, D. Horn, and E. K. Warburton, Phys. Rev. C **28**, 1171 (1983).

[11] W. Męczyński, P. Bednarczyk, R. Chapman, S. Courtin, J. Grebosz, F. Hannachi, P. Jones, J. Kownacki, M. Lach, A. Lopez-Martens, K. H. Maier, J. C. Merdinger, D. Middleton, M. Palacz, M. B. Smith, K. M. Spohr, N. Schulz, M. Zieblinski, and J. Styczen, Eur. Phys. J. A **3**, 311 (1998).
[12] M. B. Smith, R. Chapman, J. F. C. Cocks, O. Dorvaux, K. Helariutta, P. M. Jones, R. Julin, S. Juutinen, H. Kankaanpää, H. Kettunen, P. Kuusiniemi, Y. Le Coz, M. Leino, D. J. Middleton, M. Muikku, P. Nieminen, P. Rahkila, A. Savelius, and K.-M. Spohr, Eur. Phys. J. A **5**, 43 (1999).
[13] U. Jakobsson, J. Uusitalo, S. Juutinen, M. Leino, P. Nieminen, K. Andgren, B. Cederwall, P. T. Greenlees, B. Hadinia, P. Jones, R. Julin, S. Ketelhut, A. Khaplanov, M. Nyman, P. Peura, P. Rahkila, P. Ruotsalainen, M. Sandzelius, J. Sarén, C. Scholey, and J. Sorri, Phys. Rev. C **82**, 044302 (2010).
[14] H. Kettunen, T. Enqvist, M. Leino, K. Eskola, P. T. Greenlees, K. Helariutta, P. Jones, R. Julin, S. Juutinen, H. Kankaanpää, H. Koivisto, P. Kuusiniemi, M. Muikku, P. Nieminen, P. Rahkila, and J. Uusitalo, Eur. Phys. J. A **16**, 457 (2003).
[15] H. Kettunen, T. Enqvist, T. Grahn, P. T. Greenlees, P. Jones, R. Julin, S. Juutinen, A. Keenan, P. Kuusiniemi, M. Leino, A.-P. Leppänen, P. Nieminen, J. Pakarinen, P. Rahkila, and J. Uusitalo, Eur. Phys. J. A **17**, 537 (2003).
[16] M. Lach, P. Bednarczyk, P. T. Greenlees, K. Helariutta, P. Jones, R. Julin, S. Juutinen, H. Kankaanpää, H. Kettunen, P. Kuusiniemi, M. Leino, W. Męczyński, M. Muikku, P. Nieminen, P. Rahkila, J. Styczen, and J. Uusitalo, Eur. Phys. J. A **9**, 307 (2000)
[17] K. Andgren *et al.*, Phys. Rev. C **78**, 044328 (2008).
[18] S. Yashita, Ph.D. thesis, Lawrence Radiation Laboratory, Berkeley, 1983.
[19] M. Leino, Ph.D. thesis, University of Helsinki, 1983.
[20] T. Enqvist, Ph.D. thesis, University of Jyväskylä, 1996.
[21] K.-H. Schmidt, R. S. Simon, J.-G. Keller, F. P. Heßberger, G. Münzenberg, B. Quint, H.-G. Clerc, W. Schwab, U. Gollerthan, and C.-C. Sahm, Phys. Lett. B **168**, 39 (1986).
[22] R. S. Simon, K.-H. Schmidt, F. P. Heßberger, S. Hlavac, M. Honusek, G. Münzenberg, H.-G. Clerc, U. Gollerthan, and W. Schwab, Z. Phys. A At. Nucl. **325**, 197 (1986).
[23] E. S. Paul *et al.*, Phys. Rev. C **51**, 78 (1995).
[24] M. Leino, J. Äystö, T. Enqvist, P. Heikkinen, A. Jokinen, M. Nurmia, A. Ostrowski, W. H. Trzaska, J. Uusitalo, K. Eskola, P. Armbruster, and V. Ninov, Nucl. Instrum. Methods Phys. Res., Sect. B **99**, 653 (1995).
[25] R. D. Page, A. N. Andreyev, D. E. Appelbe, P. A. Butler, S. J. Freeman, P. T. Greenlees, R.-D. Herzberg, D. G. Jenkins, G. D. Jones, P. Jones, D. T. Joss, R. Julin, H. Kettunen, M. Leino, P. Rahkila, P. H. Regan, J. Simpson, J. Uusitalo, S. M. Vincent, and R. Wadsworth, Nucl. Instrum. Methods Phys. Res., Sect. B **204**, 634 (2003).
[26] R. B. Firestone eds., *Table of Isotopes, Eighth Edition* (Wiley & Sons, New York, 1996).
[27] J. Wauters, P. Dendooven, M. Huyse, G. Reusen, P. Van Duppen, and P. Lievens, Phys. Rev. C **47**, 1447 (1993)
[28] I. Lazarus *et al.*, IEEE Trans. Nucl. Sci. **48**, 567 (1995).
[29] P. Rahkila, Nucl. Instrum. Methods. Phys. Res. Sect. A **595**, 637 (2008).
[30] A. N. Andreyev *et al.*, Phys. Rev. C **79**, 064320 (2009).
[31] M. B. Smith *et al.*, J. Phys. G: Nucl. Part. Phys. **26**, 787 (2000).
[32] P. V. Duppen, P. Decrock, P. Dendooven, M. Huyse, G. Reusen, and J. Wauters, Nucl. Phys. A **529**, 268 (1991).
[33] A. Andreyev *et al.*, Eur. Phys. J. A **18**, 39 (2003).
[34] D. C. Radford, Nucl. Instrum. Methods Phys. Res. Sect. A **361**, 297 (1995).
[35] D. C. Radford, Nucl. Instrum. Methods Phys. Res. Sect. A **361**, 306 (1995).
[36] T. Chapuran, K. Dybdal, D. B. Fossan, T. Lönnroth, W. F. Piel, D. Horn, and E. K. Warburton, Phys. Rev. C **33**, 130 (1986).
[37] A. N. Andreyev, P. A. Butler, R. D. Page, D. E. Appelbe, G. D. Jones, D. T. Joss, R.-D. Herzberg, P. H. Regan, J. Simpson, and R. Wadsworth, Nucl. Instrum. Methods Phys. Res. Sect. A **533**, 422 (2004).
[38] K. Hardt, Y. K. Agarwal, C. Günther, M. Guttormsen, R. Kroth, J. Recht, F. A. Beck, T. Byrski, J. C. Merdinger, A. Nourredine, D. C. Radford, J. P. Vivien, and C. Bourgeois, Z. Phys. A At. Nucl. **312**, 251 (1983).
[39] G. Ulm, S. K. Bhattacherjee, P. Dabkiewicz, G. Huber, H.-J. Kluge, T. Kühl, H. Lochmann, E.-W. Otten, K. Wendt, S. A. Ahmad, W. Klempt, and R. Neugart, Z. Phys. A At. Nucl. **325**, 247 (1986).
[40] L. W. Nordheim, Phys. Rev. **78**, 294 (1950).
[41] C. J. Gallagher and S. A. Moszkowski, Phys. Rev. **111**, 1282 (1958).
[42] V. Paar, Nucl. Phys. A **331**, 16 (1979).
[43] M. Huyse, P. Decrock, P. Dendooven, G. Reusen, P. Van Duppen, and J. Wauters, Phys. Rev. C **46**, 1209 (1992).
[44] A. N. Andreyev *et al.*, Phys. Rev. C **73**, 024317 (2006).
[45] R. Taagepera and M. Nurmia, Ann. Acad. Sci. Fenn. A VI Physica **78**, 1 (1961).
[46] A. Andreyev, D. Ackermann, F. Heßberger, S. Hofmann, M. Huyse, I. Kojouharov, B. Kindler, B. Lommel, G. Münzenberg, R. Page, K. Van de Vel, P. Van Duppen, and K. Heyde, Eur. Phys. J. A: Hadrons Nuclei **18**, 55 (2003).
[47] H. De Witte, A. N. Andreyev, S. Dean, S. Franchoo, M. Huyse, O. Ivanov, U. Köster, W. Kurcewicz, J. Kurpeta, A. Plochocki, K. Van de Vel, J. Van de Walle, and P. Van Duppen, Eur. Phys. J. A: Hadrons Nucl. **23**, 243 (2005).
[48] J. Uusitalo, M. Leino, T. Enqvist, K. Eskola, T. Grahn, P. T. Greenlees, P. Jones, R. Julin, S. Juutinen, A. Keenan, H. Kettunen, H. Koivisto, P. Kuusiniemi, A.-P. Leppänen, P. Nieminen, J. Pakarinen, P. Rahkila, and C. Scholey, Phys. Rev. C **71**, 024306 (2005).